ARTICLES
https://doi.org/10.1038/s41561-018-0226-1

nature geoscience

Recent Southern Ocean warming and freshening driven by greenhouse gas emissions and ozone depletion

Neil C. Swart[1*], Sarah T. Gille[2], John C. Fyfe[1] and Nathan P. Gillett[1]

The Southern Ocean has, on average, warmed and freshened over the past several decades. As a primary global sink for anthropogenic heat and carbon, to understand changes in the Southern Ocean is directly relevant to predicting the future evolution of the global climate system. However, the drivers of these changes are poorly understood, owing to sparse observational sampling, large amplitude internal variability, modelling uncertainties and the competing influence of multiple forcing agents. Here we construct an observational synthesis to quantify the temperature and salinity changes over the Southern Ocean and combine this with an ensemble of co-sampled climate model simulations. Using a detection and attribution analysis, we show that the observed changes are inconsistent with the internal variability or the response to natural forcing alone. Rather, the observed changes are primarily attributable to human-induced greenhouse gas increases, with a secondary role for stratospheric ozone depletion. Physically, the simulated changes are primarily driven by surface fluxes of heat and freshwater. The consistency between the observed changes and our simulations provides increased confidence in the ability of climate models to simulate large-scale thermohaline change in the Southern Ocean.

The Southern Ocean has experienced a complex set of changes over the past several decades. There have been strong, regionally opposing trends in sea-ice since satellite observations began in 1979, with a small but significant overall increase in sea-ice cover and an associated near-surface cooling[1–3]. However, below the surface, repeat observations show a significant warming trend since 1950[4,5], and a broadscale freshening[6]. At mid depths and within the latitudes of the Antarctic Circumpolar Current, the warming has proceeded at nearly twice the rate of global upper ocean warming[4]. The processes that drive this warming make the Southern Ocean the dominant region of anthropogenic heat and carbon uptake[7–9]. Hence, to understand the drivers of these changes is vital to make reliable future climate projections[10,11], but it is complicated by several factors.

The Southern Ocean is subject to a strong internal climate variability, which may account for a substantial portion of the observed change[12–16]. It is also one of the more poorly sampled regions of the global ocean[5], which accentuates the difficulty of quantifying forced trends. Modelling results suggest that both greenhouse gas increases[17] and stratospheric ozone depletion[18,19] are important drivers of Southern Ocean change. However, the ability of coarse resolution climate models to simulate changes accurately in the Southern Ocean, in which the dynamics are modulated by small-scale eddies, has been questioned[10]. Human influence on the ocean thermohaline change has been detected previously in large-scale basin averages[20–23]. However, the observed patterns of Southern Ocean thermohaline change have not yet been attributed to specific forcing agents. Here we present a new observational synthesis of Southern Ocean temperature and salinity changes, address the questions of data sparsity and model skill, and then develop a framework to attribute these changes to individual forcing agents.

Observed and simulated changes

To quantify historical changes in the Southern Ocean temperature and salinity, we used all the hydrographic profiles available in the World Ocean Database for the period 1950–2015. We computed anomalies between each profile and the closest matching point in a modern Argo-based climatology[24] to avoid aliasing due to the sparse historical sampling, and gridded the data (see below and Methods).

The observed zonal-mean temperature change over the Southern Ocean, computed as the 2006–2015 mean minus the 1950–1980 mean, is dominated by a region of warming centred near 45 °S that extends from the surface to over 1,500 m (Fig. 1a). An interesting exception to this warming pattern is a subsurface cooling between about 250 and 2,000 m and between 30–36° S. Salinity shows a more complex pattern of change (Fig. 1b). The salinity pattern is dominated by a strong surface freshening south of 45° S, which extends into the ocean interior in a northward arc, which is contrasted against a strong salinification in the upper 500 m, north of 45° S. These patterns of change are largely consistent with previous observational studies[6,10].

To help understand these observed changes, we turned to the Canadian Earth System Model in which the ALL forcing experiment (which includes solar, volcanic, anthropogenic aerosol, ozone depletion, land use change and greenhouse gas effects (Methods)) was run 50 times from slightly different initial conditions to produce a large ensemble. The ensemble mean over the 50 realizations provides an estimate of the forced response—the fingerprint of change associated with the forcing, and the spread across the ensemble provides an estimate of the uncertainty due to internal climate variability. We subsampled the model using the same coverage of historical hydrographic profiles, determined to the nearest month, to make our results directly comparable with the observations above (Methods).

---

[1] Canadian Centre for Climate Modelling and Analysis, Environment and Climate Change Canada, Victoria, BC, Canada. [2] Scripps Institution of Oceanography, University of California San Diego, La Jolla, CA, USA. *e-mail: neil.swart@canada.ca

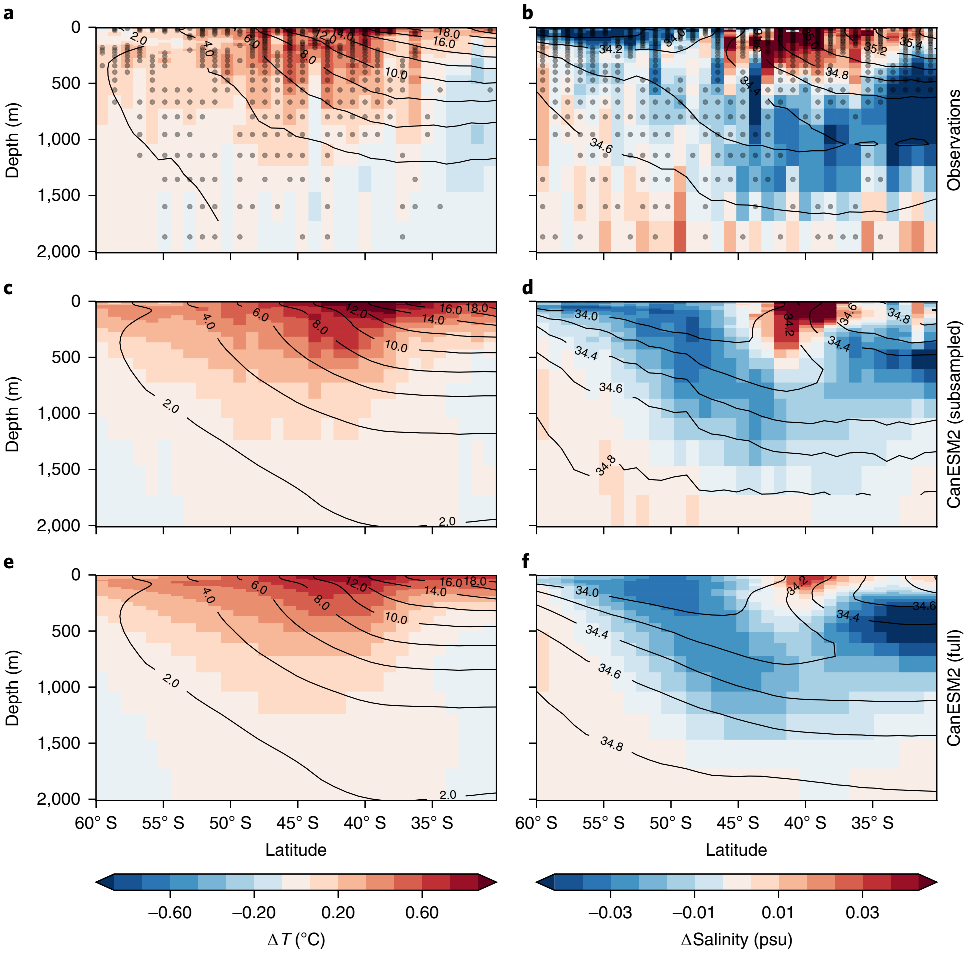

Fig. 1 | Observed and simulated changes in temperature and salinity. a–f, Zonal mean temperature (**a**, **c** and **e**) and salinity changes (**b**, **d** and **f**) from observations (**a** and **b**), the ensemble mean of the CanESM2 ALL forcing experiment, subsampled to match the observational coverage (**c** and **d**), and the ensemble mean of the CanESM2 ALL forcing ensemble with full sampling (**e** and **f**). The stipples in **a** and **b** show where the observations fall within the 2.5th to 97.5th percentile spread across the model ensemble. The anomalies represent the difference between the 2006–2015 mean and the mean over a 1950–1980 base period. Black contours are the climatological temperatures and salinities. psu, practical salinity unit.

The ALL forcing fingerprints reproduce the observed patterns of change very well (Fig. 1c,d). The correlation coefficients between the simulated and observed patterns are 0.83 and 0.72 for temperature and salinity, respectively. Regions in which the observed changes fall within the 2.5th to 97.5th percentile spread of the 50 model realizations are indicated by the stippling in Fig. 1a,b, which indicates where the model and observations agree at the 5% level. Most regions are stippled, but in the non-stippled areas the model typically correctly simulates the sign of the observed change, but does not capture the correct magnitude of the changes. In particular, the model underestimates the magnitude of the observed subsurface cooling and freshening, between about 30 to 42° S. This is partly addressed by the scaling factors introduced in the detection and attribution analysis below.

The observational coverage is extremely sparse in the early part of the record and increases over time, with a step-like jump after the introduction of the Argo array in 2004 (Supplementary Figs. 1 and 2). We can use the model to address the question of whether the sparse observational sampling biases our estimates of temperature and salinity change since 1950, despite our careful analytical approach (Methods). Figure 1e,f shows the patterns of change obtained when we use the full model coverage (no subsampling). Relative to Fig. 1c,d, in which the model was subsampled with observational coverage, we see minor differences in detail, but

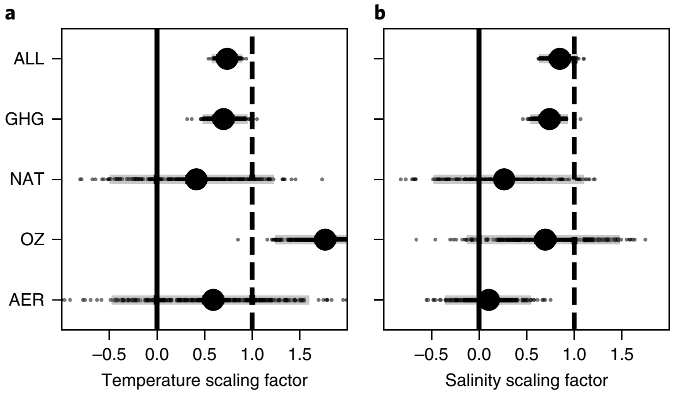

Fig. 2 | Detection and attribution scaling factors. a,**b**, Temperature (**a**) and salinity (**b**) scaling factors are shown for a one-signal analysis of the ALL forcing experiment, and for the multisignal analysis using the GHG, NAT, OZ and AER experiments. Scaling factors are the regression coefficients between the observations and the ensemble mean patterns of change for each experiment. The 90% confidence intervals (grey bars) were generated from the spread across the 200 individual realizations of the model internal variability (Methods), with the individual ensemble members shown as small black dots.

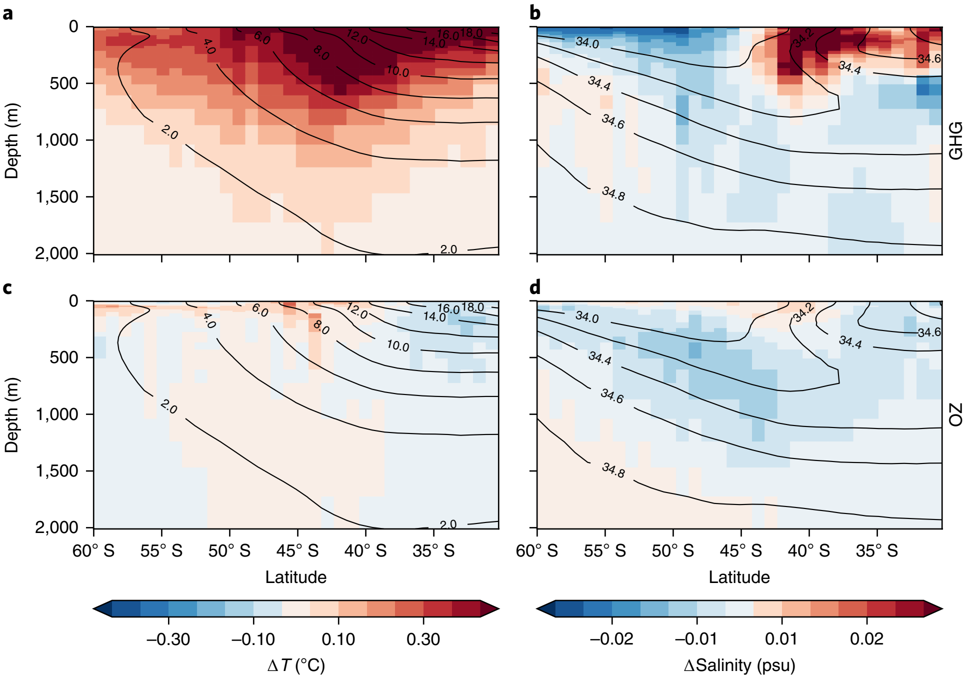

Fig. 3 | Fingerprints of temperature and salinity change. a–d, Zonal mean temperature (**a** and **c**) and salinity changes (**b** and **d**) from the ensemble means of CanESM2 single-forcing experiments using GHG and OZ, respectively. All are subsampled to match the observational coverage. The anomalies represent the difference between the 2006–2015 mean and the mean over a 1950–1980 base period. The fields are scaled to best match the observations using the scaling factors from Fig. 2

no fundamental changes in the patterns. This result suggests that the sparse observational sampling of the Southern Ocean has not systematically biased our estimates of the multidecade-scale zonal mean temperature and salinity changes. Analysis of more regional scales and a shorter period variability would, however, be increasingly subject to aliasing, and hence we did not attempt to move our analysis beyond zonal mean scales. Next, we address the drivers of these observed changes.

Detection and attribution

To objectively compare the simulated and observed Southern Ocean changes, and to determine the relative contributions of individual climate forcings to the changes, we applied a detection-and-attribution analysis[25] (Methods). We began with a one-signal analysis that regressed the observed changes (Fig. 1a,b) onto the model-derived fingerprints of change associated with the ALL forcing experiment (Fig. 1c,d). The resulting scaling factors are significantly different from zero at the 5% significance level for both temperature and salinity (Fig. 2). This means that we formally detected the fingerprints of climate change in the observed Southern Ocean temperature and salinity, and the observed changes are not explainable by internal climate variability alone[25]. The salinity scaling factor is consistent with unity, which means that the magnitude of the simulated changes is consistent with the observations. The temperature scaling factor of 0.74 does not include unity in its uncertainty range, which implies that the model response has to be scaled down to best fit the observations. This is consistent with our knowledge that the Canadian Earth System Model version 2 (CanESM2) warms too rapidly over the historical period[26].

To identify the roles of individual forcing agents, we then conducted a multisignal analysis (Methods). The fingerprints were derived from four experiments, each of which comprised 50 simulations, in which the CanESM2 model was forced by (1) greenhouse gas forcing only (GHG), (2) natural (solar and volcanic) forcing only (NAT), (3) anthropogenic aerosols only (AER) and (4) stratospheric ozone depletion only (OZ). The resulting scaling factors represent the best combined fit to the observations of the fingerprints for each individual forcing (Fig. 2). The scaling factors associated with the NAT fingerprints are not significantly different from zero, which indicates no detectable influence of the natural forcing (solar and volcanic) in these zonal mean sections. Similarly, the AER fingerprints were not detected in the observations. By contrast, we can independently detect the fingerprints of both GHG- and OZ-induced changes in the observed temperatures, whereas for salinity only the GHG fingerprint is detected. We did a combined analysis on the temperature and salinity and detected both the GHG and OZ patterns (Supplementary Fig. 3).

The relative contribution of each forcing to the observed pattern of change (Fig. 3) is given by the fingerprints multiplied by the appropriate scaling factor. For both temperature and salinity, GHG plays the dominant role (Fig. 3a,b) and shows patterns of change similar to those of the ALL forcing experiment and observations (Fig. 1). This is consistent with the understanding that increasing greenhouse gases are the principal driver of climate warming[25] and recent anomalous ocean heat uptake[27]. In our simulations, OZ is responsible for the cooling observed north of 40° S and for warming to the south (Fig. 3c), consistent with previous modelling studies[18,28,29]. The OZ response is distinct from the uniformly warming GHG signal in this regard. That the fingerprint of OZ was detected in the observations for temperature, but not of salinity, most probably lies in the fact that the GHG and OZ fingerprints are highly correlated for salinity (Fig. 3b,d), which makes independent detection difficult.

Based on these results, we conclude that the observed Southern Ocean temperature and salinity changes are inconsistent with internal variability or natural forcing alone, but can be attributed to anthropogenic influences in general, and greenhouse gas increases and stratospheric ozone depletion in particular. These results are in agreement with the previous detection of anthropogenic influence on ocean temperature and salinity at the global scale and in other

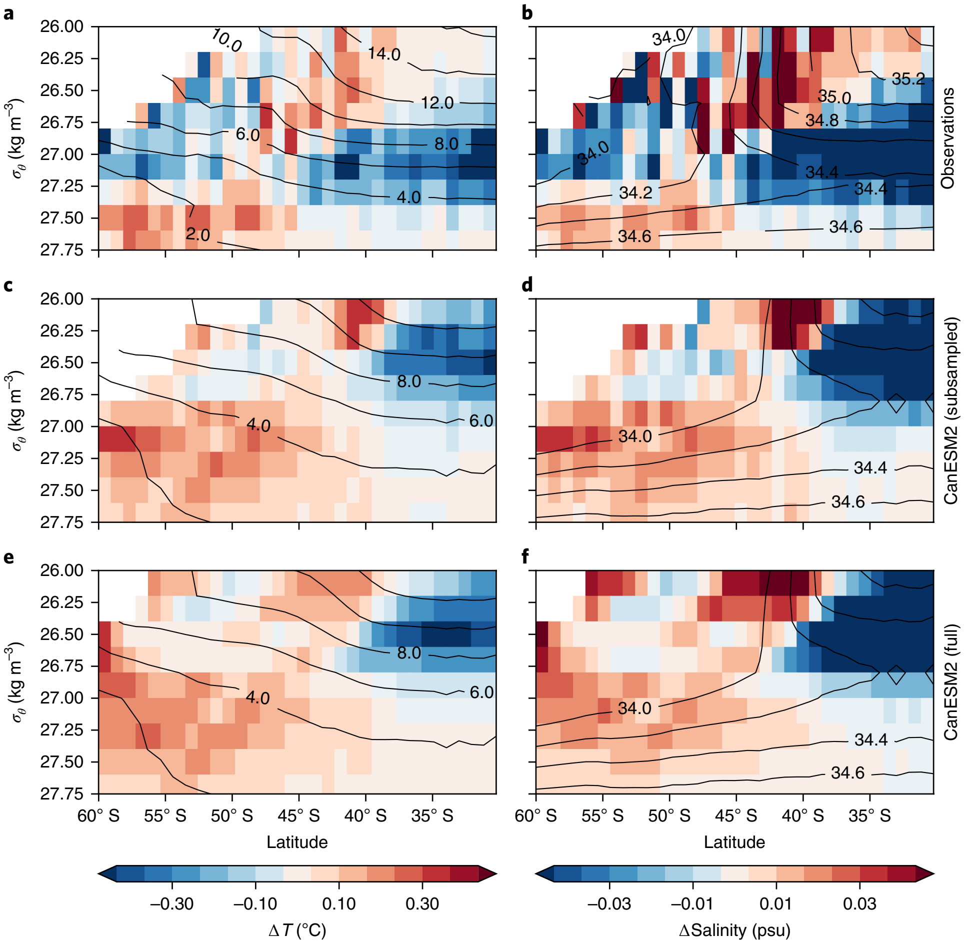

Fig. 4 | Observed and simulated changes in temperature and salinity in density space. a–f, As in Fig. 1, but with the anomalies computed in density space. Zonal mean temperature (**a**, **c** and **e**) and salinity changes (**b**, **d** and **f**) from the observations (**a** and **b**), the ensemble mean of the CanESM2 ALL forcing experiment, subsampled to match the observational coverage (**c** and **d**), and the ensemble mean of the CanESM2 ALL forcing ensemble with full sampling (**e** and **f**). The anomalies represent the difference between the 2006–2015 mean and the mean over a 1950–1980 base period. Black contours are the climatological temperatures and salinities. σ_θ is the potential density, referenced to the surface, minus 1,000 kg m^{-3}.

ocean basins[20–23]. We have advanced on previous work by using an updated observational synthesis to focus on the Southern Ocean patterns of change, and by attributing the observed changes to GHG and OZ in particular, rather than just to the combined anthropogenic signal (ALL).

Physical mechanisms

Changes in temperature and salinity on pressure surfaces (Fig. 1) can be driven by changes in surface fluxes and water masses, or by adiabatic shifts of density surfaces, which do not alter water masses (known as heave), induced by wind and ocean circulation changes. To help separate these effects, we recomputed the changes on isopycnal surfaces, $26 \leq \sigma_\theta \leq 27.75$ (σ_θ is the potential density) which comprise the main water masses of the Antarctic Circumpolar Current (Fig. 4). The observations show a warming and salinification of the Upper Circumpolar Deep Water centred on $\sigma_\theta = 27.5$, south of 45° S, and a cooling and freshening of the thermocline waters north of this and centred on $\sigma_\theta = 27.0$ (Fig. 4a,b). The CanESM2 ALL forcing simulation overall shows similar patterns of change (Fig. 4c,d), although the model does have some climatological biases in the water mass structure, and the cooling/freshening tends to occur in lighter density classes than observed. Overall, these patterns of change are consistent with previously identified water mass changes in the Southern Ocean[10,30–32] and imply water mass modification by surface fluxes.

In the model, a heat budget analysis of the ALL forcing experiment shows that 75% of the depth-integrated warming in the Southern Ocean can be explained by overlying anomalous surface heat fluxes (Fig. 5a,c). Given conservation of heat, we can infer that the remaining 25% of the simulated warming is driven by anomalous ocean heat transport across the boundaries of the domain. The salinity budget shows that most of the additional freshwater enters the ocean to the south of the boundary of our analysis area at 60° S (Fig. 5b,d), and then is advected into the analysis region by the prevailing northward Ekman transport. These results are consistent with a previous study[1], which argues that Southern Ocean warming is largely driven by anomalous surface fluxes combined with climatological transport, and that the changes in transport play only a secondary role. In our simulations, the Southern Ocean meridional overturning circulation does change (Supplementary Fig. 4), mostly driven by GHG and intensified westerly winds (Supplementary Fig. 5), whereas the Antarctic Circumpolar Current shows only a very small increase in strength (Supplementary Fig. 6).

Previous studies proposed that the observed Southern Ocean warming may be associated with poleward shifts of the Southern Ocean fronts[5,10]. The additional constraint of salinity changes suggests that this is unlikely to be the case. As salinity increases towards the north over the upper water column, the observed pattern of freshening is inconsistent with a simple southward shift of isopycnals (that is, fronts). Indeed, recent studies found no evidence that

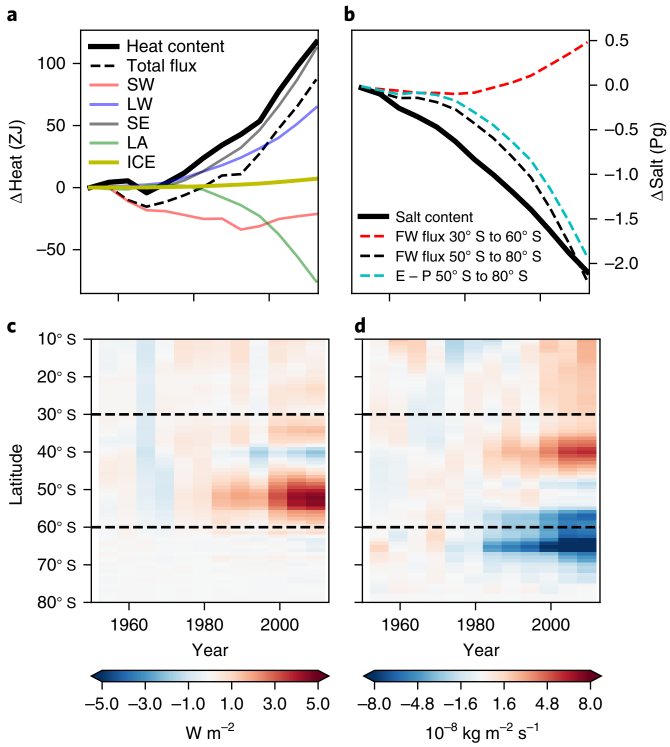

Fig. 5 | Southern Ocean heat and salt budget. a,**b**, Change in simulated Southern Ocean volume integrated (30° S to 60° S, 0–2,000 m) heat (**a**) and salt (**b**) content, along with cumulative changes in the area-integrated surface heat and (virtual) salt fluxes. **c**,**d**, Changes in zonal mean surface heat (**c**) and salt (**d**) fluxes in time over 10° S to 80° S. In **a**, contributions from shortwave radiation (SW), longwave radiation (LW) and latent heat (LA) and sensible heat (SE), and the flux below sea-ice (ICE) are shown. In **b**, E–P is evaporation minus precipitation. The dashed lines in **c** and **d** show latitudes 30° S and 60° S. The results are for the CanESM2 ALL forcing experiment.

the Southern Ocean fronts have shifted poleward[33,34]. It is also interesting that CanESM2 does not include an interactive ice sheet, but is able to simulate the observed large-scale salinity change in the Southern Ocean north of 60° S. This is evidence that the observed salinity changes are not primarily driven by freshwater input from the ice-sheet melt, which is small relative to the changes in precipitation minus evaporation[6,35,36] and northward advection of freshwater by sea-ice[37,38].

Implications for the future

Our detection and attribution analysis shows that the thermohaline changes simulated by CanESM2 are statistically consistent with the observed changes. This provides increased confidence in the ability of coarse resolution climate models (~1°) to simulate large-scale temperature and salinity changes in the Southern Ocean. Our attribution results also indicate that GHG dominated over OZ in the observed warming and freshening of the Southern Ocean since 1950 (Fig. 3). Given this, we expect to see continued warming and freshening of the Southern Ocean over the coming decades, despite the mitigating effects of ozone recovery[39,40]. Such changes are highly relevant for the future of Southern Ocean sea-ice[12,29], the Antarctic ice-sheets[41] and the global ocean uptake of heat and carbon[7–9].

Online content

Any methods, additional references, Nature Research reporting summaries, source data, statements of data availability and associated accession codes are available at https://doi.org/10.1038/s41561-018-0226-1.

Received: 9 February 2018; Accepted: 15 August 2018;

References

1. Armour, K., Marshall, J., Scott, J., Donohoe, A. & Newsom, E. Southern Ocean warming delayed by circumpolar upwelling and equatorward transport. *Nat. Geosci.* **9**, 549–554 (2016).
2. Fan, T., Deser, C. & Schneider, D. P. Recent Antarctic sea ice trends in the context of Southern Ocean surface climate variations since 1950. *Geophys. Res. Lett.* **41**, 2419–2426 (2014).
3. Parkinson, C. L. & Cavalieri, D. J. Antarctic sea ice variability and trends, 1979–2010. *Cryosphere* **6**, 871–880 (2012).
4. Gille, S. T. Warming of the Southern Ocean since the 1950s. *Science* **295**, 1275–1277 (2002).
5. Gille, S. T. Decadal-scale temperature trends in the Southern Hemisphere ocean. *J. Clim.* **21**, 4749–4765 (2008).
6. Durack, P. J. & Wijffels, S. E. Fifty-year trends in global ocean salinities and their relationship to broad-scale warming. *J. Clim.* **23**, 4342–4362 (2010).
7. Roemmich, D. et al. Unabated planetary warming and its ocean structure since 2006. *Nat. Clim. Change* **5**, 240–245 (2015).
8. Khatiwala, S., Primeau, F. & Hall, T. Reconstruction of the history of anthropogenic CO_2 concentrations in the ocean. *Nature* **462**, 346–349 (2009).
9. Frölicher, T. L. et al. Dominance of the Southern Ocean in anthropogenic carbon and heat uptake in CMIP5 models. *J. Clim.* **28**, 862–886 (2015).
10. Böning, C., Dispert, A., Visbeck, M., Rintoul, S. & Schwarzkopf, F. The response of the Antarctic Circumpolar Current to recent climate change. *Nat. Geosci.* **1**, 864–869 (2008).
11. Gent, P. R. & Danabasoglu, G. Response to Increasing Southern Hemisphere Winds in CCSM4. *J. Climate* **24**, 4992–4998 (2011).
12. Swart, N. C. & Fyfe, J. C. The influence of recent Antarctic ice sheet retreat on simulated sea ice area trends. *Geophys. Res. Lett.* **40**, 4328–4332 (2013).
13. Polvani, L. M. & Smith, K. L. Can natural variability explain observed Antarctic sea ice trends? New modeling evidence from CMIP5. *Geophys. Res. Lett.* **40**, 3195–3199 (2013).
14. Gagné, M.-È., Gillett, N. P. & Fyfe, J. C. Observed and simulated changes in Antarctic sea ice extent over the past 50 years. *Geophys. Res. Lett.* **42**, 90–95 (2015).
15. Zunz, V., Goosse, H. & Massonnet, F. How does internal variability influence the ability of CMIP5 models to reproduce the recent trend in Southern Ocean sea ice extent? *Cryosphere* **7**, 451–468 (2013).
16. Lovenduski, N. S., Fay, A. R. & McKinley, G. A. Observing multidecadal trends in Southern Ocean CO_2 uptake: what can we learn from an ocean model? *Global. Biogeochem. Cycles* **29**, 416–426 (2015).
17. Fyfe, J. Southern Ocean warming due to human influence. *Geophys. Res. Lett.* **33**, L19701 (2015).
18. Sigmond, M., Reader, M. C., Fyfe, J. C. & Gillett, N. P. Drivers of past and future Southern Ocean change: stratospheric ozone versus greenhouse gas impacts. *Geophys. Res. Lett.* **38**, L12601 (2011).
19. Solomon, A., Polvani, L. M., Smith, K. L. & Abernathey, R. P. The impact of ozone depleting substances on the circulation, temperature, and salinity of the Southern Ocean: an attribution study with CESM1(WACCM). *Geophys. Res. Lett.* **42**, 5547–5555 (2015).
20. Barnett, T. P., Pierce, D. W. & Schnur, R. Detection of anthropogenic climate change in the world's oceans. *Science* **292**, 270–274 (2001).
21. Barnett, T. P. et al. Penetration of human-induced warming into the world's oceans. *Science* **309**, 284–287 (2005).
22. Pierce, D. et al. Anthropogenic warming of the oceans: observations and model results. *J. Clim.* **19**, 1873–1900 (2006).
23. Pierce, D. W., Gleckler, P. J., Barnett, T. P., Santer, B. D. & Durack, P. J. The fingerprint of human-induced changes in the ocean's salinity and temperature fields. *Geophys. Res. Lett.* **39**, L21704 (2012).
24. Roemmich, D. & Gilson, J. The 2004–2008 mean and annual cycle of temperature, salinity, and steric height in the global ocean from the Argo Program. *Prog. Oceanogr.* **82**, 81–100 (2009).
25. Bindoff, N. et al. in *Climate Change 2013: The Physical Science Basis* (eds Stocker, T. F. et al.) (Cambridge Univ. Press, Cambridge, 2013).
26. Gillett, N. P., Arora, V. K., Matthews, D. & Allen, M. R. Constraining the ratio of global warming to cumulative CO_2 emissions using CMIP5 simulations. *J. Clim.* **26**, 6844–6858 (2013).
27. Levitus, S. et al. Anthropogenic warming of Earth's climate system. *Science* **292**, 267–270 (2001).
28. Bitz, C. & Polvani, L. Antarctic climate response to stratospheric ozone depletion in a fine resolution ocean climate model. *Geophys. Res. Lett.* **39**, L20705 (2012).
29. Sigmond, M. & Fyfe, J. C. Has the ozone hole contributed to increased Antarctic sea ice extent? *Geophys. Res. Lett.* **37**, L18502 (2010).
30. Bindoff, N. L. & McDougall, T. J. Decadal changes along an Indian Ocean section at 32° S and their interpretation. *J. Phys. Oceanogr.* **30**, 1207–1222 (2000).

31. Banks, H. T. & Bindoff, N. L. Comparison of observed temperature and salinity changes in the Indo-Pacific with results from the coupled climate model HadCM3: processes and mechanisms. *J. Clim.* **16**, 156–166 (2003).
32. Aoki, S., Bindoff, N. & Church, J. Interdecadal water mass changes in the Southern Ocean between 30° E and 160° E. *Geophys. Res. Lett.* **32**, L07607 (2005).
33. Gille, S. T. Meridional displacement of the Antarctic Circumpolar Current. *Phil. Trans. R. Soc.* **372**, 20130273 (2014).
34. Freeman, N. M., Lovenduski, N. S. & Gent, P. R. Temporal variability in the Antarctic Polar Front (2002–2014). *J. Geophys. Res. Oceans* **121**, 7263–7276 (2016).
35. Pauling, A. G., Bitz, C. M., Smith, I. J. & Langhorne, P. J. The response of the Southern Ocean and Antarctic sea ice to freshwater from ice shelves in an Earth system model. *J. Clim.* **29**, 1655–1672 (2016).
36. Fyfe, J. C., Gillett, N. P. & Marshall, G. J. Human influence on extratropical Southern Hemisphere summer precipitation. *Geophys. Res. Lett.* **39**, L23711 (2012).
37. Abernathey, R. et al. Water-mass transformation by sea ice in the upper branch of the Southern Ocean overturning. *Nat. Geosci.* **9**, 596–601 (2016).
38. Haumann, A., Gruber, N., Münnich, M., Frenger, I. & Kern, S. Sea-ice transport driving Southern Ocean salinity and its recent trends. *Nature* **537**, 89–92 (2016).
39. Polvani, L. M., Previdi, M. & Deser, C. Large cancellation, due to ozone recovery, of future Southern Hemisphere atmospheric circulation trends. *Geophys. Res. Lett.* **38**, L04707 (2011).
40. Previdi, M. & Polvani, L. M. Climate system response to stratospheric ozone depletion and recovery. *Q. J. R. Meteorol. Soc.* **140**, 2401–2419 (2014).
41. Pritchard, H. D. et al. Antarctic ice-sheet loss driven by basal melting of ice shelves. *Nature* **484**, 502–505 (2012).

Acknowledgements

We acknowledge the Environment and Climate Change Canada's Canadian Centre for Climate Modelling and Analysis for executing and making available the CanESM2 Large Ensemble simulations used in this study, and the Canadian Sea Ice and Snow Evolution Network for proposing the simulations. S.T.G. acknowledges NSF awards PLR-1425989 and OCE 1658001.

Author contributions

N.C.S. conducted the analysis the wrote the paper. S.T.G. obtained and preprocessed the observational data. J.C.F. proposed the paper. N.P.G. advised on the detection and attribution. All the authors contributed to the scientific interpretation of the results, and helped to edit the paper.

Competing interests

The authors declare no competing interests.

Additional information

Supplementary information is available for this paper at https://doi.org/10.1038/s41561-018-0226-1.

Reprints and permissions information is available at www.nature.com/reprints.

Correspondence and requests for materials should be addressed to N.C.S.

Methods

Observations. As the observational record is sparse, particularly in the early part of the record (Supplementary Fig. 1), we need to compute anomalies carefully to avoid aliasing. For a reliable baseline, we used the well-sampled modern Argo era (2004–2008), specifically the gridded Roemmich and Gilson (RG) Argo based climatology[24], which is available at http://sio-argo.ucsd.edu/RG_Climatology.html. For every historical profile available in the World Ocean Database (https://www.nodc.noaa.gov/OC5/WOD/pr_wod.html) for the period 1950–2015, we computed the temperature and salinity anomaly relative to the RG climatological value for the same month, and the closest position in space to the profile. Computing anomalies in such a manner is used to avoid seasonal and spatial aliasing effects that result from averaging sparse observations[10]. We then bin averaged these observed anomalies in space onto the CanESM2 model grid, with a nominal resolution of 1° in latitude and 1.5° in longitude and at a time resolution of one month. After using this monthly resolved data to define the subsampling of the model (see below), we further averaged to 5-yr means. Finally, we computed the differences between the mean over the decade 2006–2015 minus the base period, which is a mean over 1950–1980.

CanESM2 large ensembles. We used CanESM2[42,43], the version of the model used for the Coupled Model Intercomparison Project Phase 5 (CMIP5). The model consists of the CanAM4 atmosphere model, run at a T63 spectral resolution and coupled to the CanOM4 ocean model, which has a nominal resolution of 1° in latitude and 1.5° in longitude. CanESM2 includes a land surface scheme (CLASS) and interactive carbon cycle components on the land (CTEM) and in the ocean (CMOC).

Four CMIP5 attribution experiments were conducted with the model: (1) ALL, (2) NAT, (3) AER and (4) OZ. In all cases, the model was run over the historical period (1950–2005) joined with future runs using the appropriate forcing from the Representative Concentration Pathway (RCP) 8.5 (2006–2100). We are only interested in the period that extends from 1950 to 2015. There is very little difference between the RCPs between 2006 and 2015. For each experiment, the initial condition in 1950 is taken from the five CanESM5 realizations submitted to the CMIP5 archive. In this year, the five realizations were branched into 50 realizations per experiment (for a total of 200), by introducing a random permutation to the seed used in the random number generator for cloud physics, which was then integrated forwards under the appropriate historical or RCP8.5 forcing. No other perturbation was made to the realizations, but the subtle change to the random seed for cloud physics ensures that internal variability diverges rapidly across the realizations. Therefore, within each experiment, the forcing is identical, and the runs only differ in their realization of internal variability.

A large ensemble was not run with GHG, but we are interested in the impacts of GHGs alone. The difference between the all forcing experiment and the sum of the other three provides an estimate of the influence of greenhouse gases, under the assumption that the responses to these forcings sum linearly (that is $\mathrm{ALL} = \mathrm{GHG} + \mathrm{NAT} + \mathrm{OZ} + \mathrm{AER}$). We can verify that this assumption holds by comparing to five CanESM2 simulations forced by GHG, which were submitted to CMIP5. The ensemble mean response to GHG inferred from the large ensembles, using the assumption of linearity above, is nearly identical to the ensemble mean response in the five actual GHG simulations (Supplementary Fig. 7).

In the model at each spatial point and for each month, we computed anomalies relative to the model climatology over 2004 to 2008 (the same period used to compute the RG observed climatology—the model and RG baseline climatologies both have complete spatial coverage). The observations have many grid points that contain no data. We used the missing data mask from the observations and applied it to the model, so that data coverage was exactly consistent between them. After this point, all the averages were applied in the same way to the model and observations, which ensured consistent sampling. Specifically, we bin averaged the data into 5-yr means, and then we computed the differences between the mean over the decade 2006–2015 minus the base period, which is the mean over 1950–1980.

Although the large size of the CanESM2 ensemble provides robust estimates of the forced response (fingerprints), and the range of internal variability, it does not sample model uncertainty. However, the warming pattern in CanESM2 is consistent with the average across the CMIP5 models[1].

Detection and attribution methodology. In the context of our study, detection means to demonstrate that the Southern Ocean temperature and salinity have changed in a statistical sense, and that this change is inconsistent with internal variability. Attribution means to determine the relative contributions of multiple climate forcings to the change, with an assigned statistical confidence[25]. Attribution to a specific forcing is done by showing that the observed changes are consistent with the process-based model (CanESM2), which includes the forcing (for example, greenhouse gas increases), but is inconsistent with an otherwise identical model that excludes this forcing.

We adopted the widely used fingerprinting approach, which means that we assumed that the model simulates the pattern (or fingerprint) of the response to external forcing, but not necessarily the correct magnitude of the response[25]. For each of the experiments (ALL, GHG, NAT, AER and OZ), the fingerprint is the ensemble mean over 50 model realizations, which differ only in their rendition of internal variability. The analysis produces scaling factors that describe how the magnitude of the model response to individual forcings should be scaled up or down to best match the observations and associated uncertainty estimates[25].

To obtain the scaling factors, we regressed the observed changes onto the simulated fingerprint(s). In the one-signal case, the observations were regressed on the ALL forcing fingerprint. In the multisignal case, a multiple linear regression was used to regress the observations onto the fingerprints for each of the four experiments. As the simulated forced response is estimated from the ensemble mean of a 50-member ensemble, internal variability in the forced response is negligible, and so we used an ordinary least squares regression[25].

To estimate uncertainty of the coefficients, we computed the residual between each realization and the ensemble mean from its experiment, which provides us with 200 realizations of internal variability. We rescaled the realization by $\sqrt{50/49}$ to account for subtraction of the ensemble mean[44]. We then repeated the regressions 200 times, in each iteration replacing the observations with a different realization of the variability. That is, we regressed the realization of internal variability against the ensemble means. The spread (5th to 95th percentile) in parameters derived in this way provides the uncertainty in the scaling factors, and informs us of the likelihood of obtaining the scaling factors due to internal variability alone. This confidence interval allows us to evaluate if the scaling factors are significantly different from zero at the 5% level. For display purposes, in Fig. 2 we centre this distribution of scaling factors on the corresponding regression coefficient of the forced response. Our approach leverages the large number of independent samples of internal variability available to avoid the need to estimate uncertainty intervals from an ill-conditioned covariance matrix and to avoid assuming normally distributed internal variability, as has been done previously[22].

Using different variables that are physically linked, such as temperature and salinity, can increase the signal detectability[23]. For the combined temperature and salinity analysis (Supplementary Fig. 3), the temperature and salinity fingerprints used above were normalized (that is, the mean was removed and they were divided by the standard deviation). The data were then concatenated (to produce a series double the length of the temperature or salinity data alone), and the above analysis was repeated.

Code availability. The analysis code is available from the authors upon request.

Data availability

All the data used in this article are publicly available. The CanESM2 large ensembles are available at http://open.canada.ca/data/en/dataset/aa7b6823-fd1e-49ff-a6fb-68076a4a477c. The RG Argo climatology is available at http://sio-argo.ucsd.edu/RG_Climatology.html. The historical profiles from the World Ocean Database can be found at https://www.nodc.noaa.gov/OC5/WOD/pr_wod.html.

References

42. Arora, V. K. et al. Carbon emission limits required to satisfy future representative concentration pathways of greenhouse gases. *Geophys. Res. Lett.* **38**, L05805 (2011).
43. Yang, D. & Saenko, O. A. Ocean heat transport and its projected change in CanESM2. *J. Clim.* **25**, 8148–8163 (2012).
44. Stone, D., Allen, M. R., Selten, F., Kliphuis, M. & Stott, P. A. The detection and attribution of climate change using an ensemble of opportunity. *J. Clim.* **20**, 504–516 (2007).